Investigation of potential extreme load reduction for a two-bladed upwind turbine with partial pitch

Kim, Taeseong; Larsen, Torben J.; Yde, Anders

Published in:
Wind Energy

Link to article, DOI:
10.1002/we.1766

Publication date:
2015

Document Version
Publisher's PDF, also known as Version of record

Wind Energy

WIND ENERGY
Wind Energ. (2014)
Published online in Wiley Online Library (wileyonlinelibrary.com). DOI: 10.1002/we.1766

RESEARCH ARTICLE

Investigation of potential extreme load reduction for a two-bladed upwind turbine with partial pitch

Taeseong Kim, Torben J. Larsen and Anders Yde

Technical University of Denmark, Department of Wind Energy, Roskilde 4000, Denmark

ABSTRACT

This paper presents a wind turbine concept with an innovative design combining partial pitch with a two-bladed (PP-2B) turbine configuration. Special emphasis is on extreme load reduction during storm situations at standstill, but operational loads are also investigated. In order to compare the loads and dynamics of the PP-2B turbine, a partial pitch three-bladed (PP-3B) turbine and a normal pitch regulated three-bladed (3B) turbine are introduced on the basis of solidity similarity scaling. From the dynamic comparisons between two- and three-bladed turbines, it has been observed that the blade vibrations are transferred differently from the rotor to the tower. For a three-bladed turbine, blade vibrations seen in a fixed frame of reference are split with ±1P only. A two-bladed turbine has a similar split of ±1P but also includes contributions on higher harmonics (±2P, ±3P, … etc.). Further on, frequency split is also seen for the tower vibrations, where an additional ±2P contribution has been observed for the two-bladed turbine. Regarding load comparisons, the PP-2B turbine produces larger tower load variations because of 2P excitation during the operational cases. However, extreme loads are reduced by approximately 20% for the PP-2B and 18% for the PP-3B compared with the 3B turbine for the parked condition in a storm situation. Moreover, a huge potential of 60% is observed for the reduction of the extreme tower bottom bending moment for the PP-2B turbine, when the wind direction is from ±90° to the turbine, but this also requires that the turbine is parked in a T-configuration. © 2014 The Authors. Wind Energy published by John Wiley & Sons, Ltd.

KEYWORDS

extreme load reduction; partial pitch two-bladed turbine; load comparisons; dynamics comparisons; solidity similarity scaling

Correspondence

T. Kim, DTU Wind Energy, Roskilde, 4000, Denmark.
E-mail: tkim@dtu.dk

Received 30 August 2013; Revised 23 April 2014; Accepted 27 April 2014

NOMENCLATURE

A	cross-section area
c	outer chord length of cross-section
c_i	inner chord length of cross-section
h	outer height of cross-section
h_i	inner height of cross-section
I_x	area moment of inertia about the x axis (flapwise stiffness component)
I_y	area moment of inertia about the y axis (edgewise stiffness component)
M	moment
R, r	radius
S	solidity
SF	scaling factor
t	thickness of cross-section
W	sectional modulus
σ	stress

1. INTRODUCTION

Even though three-bladed turbines are the most commonly known and produced type of turbines, it is not evident that this concept in all situations is the most cost-effective turbine concept. Ever since the early days of the wind energy industry in the 1970s and 1980s, several different concepts have been tested.[1–6] Many of these showed either to be difficult to scale up in size or simply to be less cost-effective than the three-bladed concepts. In the 1990s, the discussion was mainly focusing on whether the most cost effective turbine concept was using stall or pitch control but still related to horizontal axis three-bladed wind turbines. When variable generator control was introduced in combination with blade pitch control, the benefits related to power quality and aerodynamic damping of structural vibrations seemed to outperform the stall and active stall controlled turbines. The largest active stall controlled turbine produced was the Siemens 2.3MW introduced in 2003. Now, the discussion regarding large multi-megawatt turbines is mainly focused on whether it should be produced with or without direct drive technology, hence without a main gearbox, but significant changes as to the design are only rarely challenged. As for special offshore conditions on deep water, a small increase in the interest of vertical axis wind turbines has been seen,[7] but these turbines have not yet entered into the market and are so far primarily of research interest. Three-bladed pitch controlled turbine still seems to be the way to succeed.

Parallel to the continuous development of three-bladed turbines, two-bladed turbines have been developed and investigated as well. The National Aeronautics and Space Administration (NASA),[3–5] Sandia,[8] Risø National Laboratory of Denmark,[9–13] National Renewable Energy Laboratory (NREL)[14] and others have looked into the possibility of using two-bladed horizontal axis wind turbines. The motivation for this has been related to lower weight, one blade less, and a potential for lower loads levels than for a similar three-bladed configuration. Especially, the teeter bearing known from two-bladed helicopters could cause a significant load reduction on the blades, which could potentially enable an increased rotor diameter, hence larger power production.[11,12] However, the disadvantages of the teeter concept were mainly the increased costs and complexity of the teetering hub.

Recently, the question of best cost efficiency between two- and three-bladed turbines has been brought up again by Envision. This concept is interesting since it is based on a two-bladed, rigid hub and a partial pitch blade design. The two-bladed design could in itself reduce extreme loads in storm situations, since it can be parked in a horizontal T-configuration, hence having a very limited frontal area toward the wind. With the rigid hub, the mechanical design is way less complicated than for a teetered configuration, but this could be on the expense of large dynamic loads during operation - this still has to be investigated. A blade design with partial pitch is also a new and innovative solution, which may have advantages on the turbine load level. The inner part is being stall controlled, and the outer part is pitch controlled. The purpose of this paper is, on a rational basis, to compare the advantages and disadvantages of a partial pitched two-bladed turbine (PP-2B) concept and compare with a similar three-bladed pitch (3B) and partial pitch (PP-3B) variable speed concept.

2. METHOD

The study in this paper is based on numerical analysis using the aeroelastic software HAWC2, developed at Risø National Laboratory of Denmark (Now DTU Wind Energy). The structural part of the code is a multibody formulation based on the floating frame of reference method as described in Refs. 15 and 16. In the particular formulation of the code, the turbine structure is subdivided into a number of bodies where each body has its own coordinate system. Within each body, the structure consists of an assembly of linear Timoshenko beam elements. The nonlinear effects of the body motion (rotations and deformations) are accounted for in the coupling constraints in between the individual bodies, ensuring small deflections within the linear beam elements. This means that effects of large rotations and deflections are included using a proper subdivision of a blade to a number of bodies. The suggested method has been validated with another existing nonlinear multibody formulation with the classical spin-up maneuver example.[16] The aerodynamic part of the code is based on the blade element momentum (BEM) theory, however extended from the classic steady state description to handle dynamic inflow, dynamic stall, skew inflow and effects from operating in sheared inflow. The dynamic stall model[18] consists of a modified Beddoes–Leishmann model[19] that includes the effects from shed vorticity from the trailing edge[20] and the effects of stall separation lag caused by an instationary trailing edge separation point. Variations in the induction over the rotor, caused by operation in sheared inflow are described in Ref. 21. The inflow turbulence is generated using the Mann model,[22] which is a non-isotropic full 3D correlated turbulent flow field corresponding to the Navier–Stokes solution of a turbulent flow. Tower shadow effects are included using a potential flow method. The code verification has been performed through the Offshore Code Comparison Collaboration (OC3) and Offshore Code Comparison Collaboration Continuation (OC4) under the International Energy Agency (IEA) Wind Task where HAWC2 results are validated against other numerical tools such as BLADED, ADAMS, FAST, FLEX and so on.[23,24] The full system natural frequencies, dynamic loads and displacements are compared in OC3 and OC4. From the comparisons, it has been shown that the full system natural frequencies, the dynamic loads and the system responses obtained by HAWC2 agree well with other aeroelastic codes. A full-scale validation of simulated and measured wind turbine load levels have recently been presented in Ref. 17

showing a very good agreement. The simulation time is typically between real time and two times slower than real time depending on the turbine and situation analyzed.

3. MODEL DESCRIPTION

Three different turbine configurations are considered: a PP-2B turbine, a partial pitch three-bladed (PP-3B) turbine and a normal pitch three-bladed (3B) turbine. The blade models for the three-bladed turbines, PP-3B and 3B, are scaled directly from the PP-2B on the basis of principals shown in Ref. 12. In order to ensure identical aerodynamic properties between the two- and three-bladed turbines, the scaling is performed using identical solidity for the turbines. This means that the chord length of the two-bladed turbine is 1.5 times the chord of the three-bladed one, which again means that the aerodynamic power performance should be identical except for deviations caused by the tip loss effects.

3.1. The PP-2B turbine

The PP-2B was introduced by Envision (Figure 1). The blade is divided in two parts referred to as the inner and outer parts with a total length of 62 m. The inner part, with a length of 20 m, is fixed to the hub and is designed for stall regulated performance. The outer part, with a length of 42 m, is connected to the inner blade part with a pitch bearing and is designed for pitch-regulated operation with a significantly higher lift to drag ratio than the inner part. Both inner and outer parts of the blade were made of reinforced glass fiber composites.

There are several motivations for having partial pitch blade design. One is to improve transport, installation and other practical issues of handling very large-sized blades, but the main advantage of the partial pitch concept is that the entire blade in standstill or operation above rated power never has full lift or full drag condition at the same time. This is illustrated in Figure 2, where the aerodynamic forces of a full-span blade are compared with a partial pitch. A conventional blade will, in some situations, be exposed to either full lift or full drag over the blade span depending on the wind direction. With a partial pitch blade, full lift or drag will not occur at the same time, which ensures a load alleviating effect. Since the inner and outer parts have almost same surface area, the loads from each part are of same magnitude during a standstill condition. This means that loads transferred to the hub and further down to the tower and foundation could potentially be reduced significantly compared with the conventional full span pitch concept.

3.2. The PP-3B turbine

The blade model used for the PP-3B turbine is scaled directly from the PP-2B blade. The scaling ensures that the overall aerodynamic power of the blade is identical for the two turbines except for the tip loss effect.[2,25] The tip loss correction was originally derived for a vortex sheet behind a horizontal axis rotor and includes two contributing effects. The first effect is the flow around the tip from the pressure to the suction side, which ensures that the loading at the tip is zero. The second effect is from the finite number of blades, where the axial flow velocity is higher between the blades than around the blades. With only few blades, a higher flow variation occurs, which again causes a slightly lower thrust on the rotor and aerodynamic power production for a two- and three-bladed wind turbine. By increasing the thrust on the two-bladed rotor, it is possible to regain the power loss, but in order to simplify the study, we have chosen to keep both the solidity and the rotor speed identical for the two- and three-bladed turbines. This enables a simple scaling but more importantly that the same turbine controller can be used for both concepts.

(a) Normal operation condition below rated wind speed, where the pitch of the inner and outer blade part are aligned.

(b) Parked condition where the outer parts of the blades are pitched 90°.

Figure 1. Conceptual images of the PP-2B turbine.

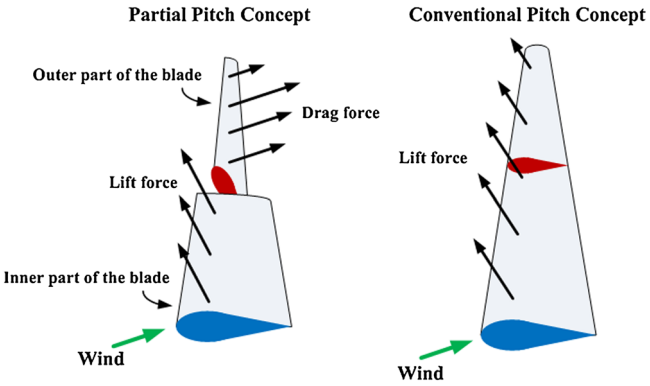

Figure 2. A sketch of the partial pitch blade strategy.

The radially dependent solidity S is defined

$$S = \frac{N c(r)}{2\pi r} \tag{1}$$

where N is number of blades, c is the chord length and r is the local blade radius, respectively.

By requiring a similar solidity for the two- and three-bladed turbines, it is seen from equation (1) that the chord of the three-bladed turbine should be scaled with a factor (SF) of 2/3, corresponding to the blade number ratio.

$$c_{3B}(r) = \frac{2}{3} c_{2B}(r) \tag{2}$$

The blade stiffness and geometry related values such as thickness of the cross-section, shear center, elastic center, height of the cross-section and so on, must be changed accordingly with the scaling factor (2/3). In this paper, it is assumed that the structural properties of the blade are obtained by the rectangular main spar cross-sectional properties, illustrated in Figure 3.

The moment of inertia I_x and I_y of the rectangular cross-section can be computed as follows:

$$I_x = \frac{1}{12}\left(c h^3 - c_i h_i^3\right), \quad I_y = \frac{1}{12}\left(h c^3 - h_i c_i^3\right) \tag{3}$$

which can be further expanded to

$$I_x \approx \frac{1}{2} c h^2 t + \frac{1}{6} h^3 t,\ I_y \approx \frac{1}{2} h c^2 t + \frac{1}{6} c^3 t \tag{4}$$

where higher order terms of t are ignored.

When scaling the cross-sectional properties between a two- and a three-bladed turbine, the material stress level should remain similar. These stresses are simply calculated in equation (5) for a simple load carrying beam.

$$\sigma_{2B} \equiv \sigma_{3B} \tag{5}$$

which is rewritten to

$$\frac{M_{2b}}{W_{2b}} \equiv \frac{M_{3b}}{W_{3b}} \tag{6}$$

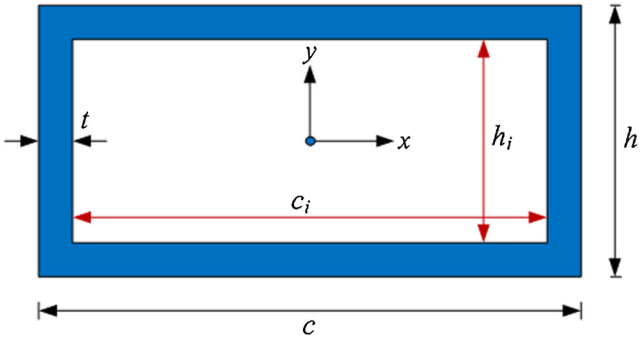

Figure 3. A sketch of cross section of the blade main spar.

where M represents moment and W means the moment of resistance. The moment of resistance of the rectangular section is for a simple beam

$$W = \frac{I}{0.5h} \tag{7}$$

Since the chord (c) and the height (h) of the PP-3B are 2/3 of the PP-2B, $c_{3b} = 2/3c_{2b}$ and $h_{3b} = 2/3h_{2b}$, and the rotor speed is identical, a direct first order consequence is that the blade loads for the PP-3B turbine are 2/3 times smaller than for the PP-2B turbine. In this case, equation (6) can be reduced to

$$W_{3b} = \frac{2}{3} W_{2b} \tag{8}$$

The thickness of the cross-section is obtained by substituting equations (4) and (7) into equation (8), which results in the thickness relation

$$t_{3b} = \frac{3}{2} t_{2b} \tag{9}$$

which means that the geometrically larger profile for the PP-2B also consists of significantly lower material thickness, even though the load is 3/2 larger than the PP-3B.

The resulting ratio between moment of inertia for the PP-2B and PP-3B turbines can be obtained by substituting equation (9) into equation (4).

$$I_{x_{3b}} = \left(\frac{2}{3}\right)^2 I_{x_{2b}} \tag{10}$$

From equation (9), the ratio between areas of the cross-sections can be computed as well

$$A_{3b} \approx 2(c_{3b} + h_{3b})\, t_{3b}, \quad A_{2b} \approx 2(c_{2b} + h_{2b})\, t_{2b} \Rightarrow A_{3b} = A_{2b} \tag{11}$$

Assuming that the blade cross-sectional weight is proportional to the area of the spar, the total weight of one blade for the PP-3B turbine is the same as for one blade of the PP-2B turbine, which again results in a potential weight reduction of the rotor by 1/3 using two blades instead of three.

3.3. The 3B turbine

On the basis of the scaling principles listed in the previous text, blade data for the PP-3B turbine is generated. Slight modifications of the mass distribution near the pitch bearing were necessary because of the changed size and location of the pitch bearing. The PP-2B has the pitch bearing from 19.68 to 20 m from the blade root. Therefore, additional mass is distributed in the root area of the 3B.

4. NUMERICAL RESULTS

In this section, the natural frequencies of three different turbines are compared at standstill and for a rotating turbine. Operational and extreme loads from the PP-2B turbine are compared according to a condensed selection of design load cases (DLCs) from IEC61400-1.[26] Moreover, some principal differences in turbine dynamics between two- and three-bladed turbines are also investigated.

4.1. Comparison of natural frequencies

The isolated blade natural frequencies of the three different turbines are compared, shown in Table I. As mentioned previously, the blade for the three-bladed turbines has been scaled using the solidity similarity, and the stress level is also similar for the two- and three-bladed turbines. Therefore, the blade structural stiffness for the three-bladed turbine is $(2/3)^2$ times softer than for the two-bladed turbine, whereas the blade weight for all three turbines are the same. The natural frequencies for the three-bladed turbine are approximately 2/3 times lower than for the two-bladed. The natural frequency comparison of the turbines is shown in Table II. The tower related frequencies for the two-bladed turbine is higher than the three-bladed. This is caused by a lower rotor weight for the two-bladed turbine than for the three-bladed turbine.

Table I. Blade natural frequency comparisons.

Mode	Description	PP-2B	PP-3B	3B
1	First flap mode	0.71	0.47	0.47
2	First edge mode	1.13	0.75	0.75
3	Second flap mode	1.70	1.14	1.13
4	Second edge mode	2.89	1.99	2.02
5	Third flap mode	3.06	2.05	2.07

Table II. Whole turbine natural frequency comparisons.

Mode	Description for two-bladed turbine	PP-2B (T-conf.)	PP-2B (I-conf.)	Description for three-bladed turbine	PP-3B	3B
1	Tower fore-aft mode	0.28	0.27	Tower fore-aft mode	0.26	0.25
2	Tower side-side mode	0.28	0.28	Tower side-side mode	0.27	0.26
3	First blade assym. flap mode	0.61	0.69	First blade assym. flap yaw	0.45	0.45
4	First blade col. flap mode	0.72	0.72	First blade assym. flap pitch	0.47	0.46
5	First blade symm. edge mode	1.12	1.15	First blade col. flap	0.49	0.48
6	Second blade asymm. flap mode	1.24	1.46	First blade assym. edge pitch	0.75	0.75
7	Second blade col. flap mode	1.74	1.74	First blade assym. edge	0.77	0.76

assym. = asymmetric; col. = collective; symm. = symmetric; T-conf. = T-configuration; I-conf. = I-configuration.

4.2. Comparison of structural frequencies during operation

The structural frequencies of a wind turbine are changed when changing the rotor speed, which is mainly caused by gyroscopic and centrifugal effects.[27,28] These effects are included in all modern aeroelastic codes,[15,29–32] but only few codes are capable of handling this in linearized models used for analyzing the mode shapes and frequency of an operating turbine; DTU Wind Energy has developed the linearized aeroelastic code for designing controllers and investigating stability problems of three-bladed turbines, called HAWCStab2.[33] When it comes to two-bladed turbines, it is even more difficult to create valid linearized models, since the rotor dynamics vary with rotor position and is therefore highly periodic. Methods do exist to overcome this, using, e.g., Floquet theory,[34,35] but so far, this is not implemented in HAWCStab2. The rotational effects have instead been investigated using frequency analysis of time domain simulations. The turbine is rotating with a prescribed rotor speed. Aerodynamics are neglected, and the turbine structure has been excited with random impulse forces on the tower top and at two different positions on the blades (in both axial and tangential direction) to properly excite tower and rotor modes. A Campbell diagram was created by frequency analysis of the tower top bending moment and force, $\sqrt{M_x^2 + F_z^2}$, and plotted with a special waterfall plot technique. In order to validate the suggested approach, a Campbell diagram for the 3B turbine is obtained from HAWC2 time simulations and compared with results calculated by HAWCStab2 (Figure 4).

It can be seen in Figure 4 that the suggested method (Figure 4(b)) compared with HAWCStab2 result (Figure 4(a)) is able to predict the structural frequencies of the low modes during the operation up to a level of 1.3 Hz. The first tower modes and the first flap and edge-related rotor modes agree very well. The ±1P is also visible in both the analytical and time domain-based plot. Using the same method, the structural frequencies of the PP-2B turbine is investigated (Figure 5).

In Figure 5, a similar Campbell diagram was constructed on the basis of time domain simulations. A significantly different pattern of frequency splitting is seen for the two-bladed turbine compared with the three-bladed turbine. The forward and backward flap and edge whirl modes are spread with not only ±1P frequency but also multiple P frequency (higher harmonics). The tower frequency is also spread with ±2P frequency (Figure 5(b)), which does not occur for the three-bladed turbine. It is also interesting to notice that for low rotational speeds, it is very difficult to distinguish the individual blade whirling frequencies. It is a larger area with many frequencies and higher harmonics appearing differently for different rotor azimuth positions in the change between I-configuration (marked □ at standstill frequency) and T-configuration (marked ○ at standstill frequency) frequencies. From the Campbell diagram of the PP-2B, it seems that there are limited design space at the operation speed range because of multiple P frequency excitations. However, all frequencies may not be critical because it depends on the correct amount of aerodynamic damping for the individual frequency. On the basis of this result, it is now possible for other two-bladed turbines to predict the operational frequencies. The frequencies split with ±1P, ±2P, … and so on. where the base frequency from this split is the mean value of the frequency pairs from turbine modes at different azimuth positions.

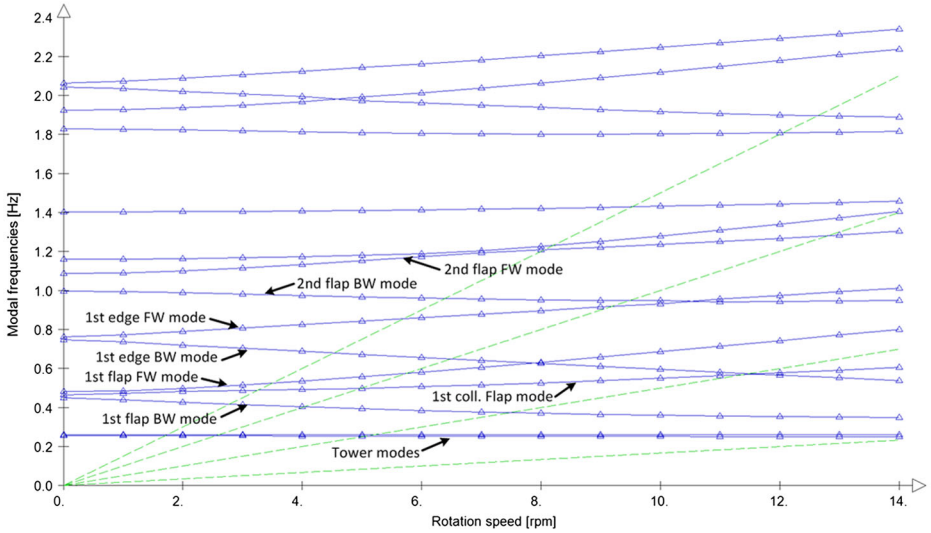

(a) Campbell diagram obtained by HAWCStab2; green lines are representing 1P, 3P, 6P, and 9P, respectively.

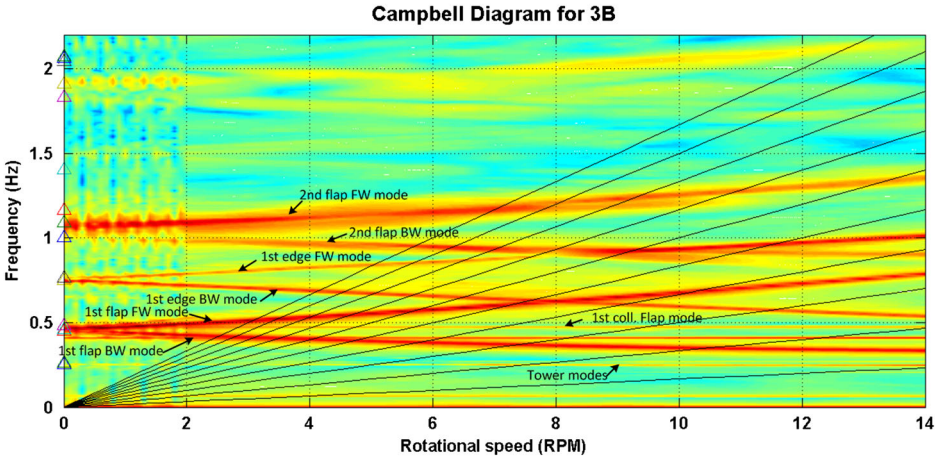

(b) Campbell diagram obtained by HAWC2; Δ represents modes at standstill.

Figure 4. Structural frequency comparisons between HAWCStab2 and HAWC2; the forward (FW) and backward (BW) flap and edge whirl modes are spread with ±1P.

4.3. Comparison of turbine dynamics between Two- and Three-bladed turbines

Dynamics of wind turbines on two- and three-bladed turbines are on several areas different from each other. First of all, the dominating load input frequency from the rotor is 2P for a two-bladed and 3P for a three-bladed wind turbine, which is illustrated in Figure 6. The rotational sampling of turbulence results in blade load input on 1P and higher harmonics, which is the same for both two- and three-bladed turbines. Secondly, the structural dynamics is different as stated in Section 4.2.

Figure 6 shows the PP-2B and the 3B turbine tower bottom fore-aft and blade root flapwise bending moment in time and frequency domain. Both cases are simulated with normal turbulence (turbulence intensity of 18%) condition at $11\,\mathrm{m\,s^{-1}}$. All results are normalized with an absolute value of the minimum out-of-plane blade root bending moment of the PP-2B at $11\,\mathrm{m\,s^{-1}}$ (Figure 11). The 2P and 3P multiple excitation frequencies on the tower are clearly seen from the figures. The blade root flapwise bending moment from PP-2B is bigger than 3B because the PP-2B has one blade less for carrying the loads. The blade root bending moment might be reduced by using a teeter-hinged hub.

A special situation demonstrating the difference related to gyroscopic effects of two- and three-bladed turbines is during yaw operation of the turbine. It is well known that the gyroscopic effects have a larger impact on a two-bladed turbine compared with a three-bladed.[36] The size of these effects depends on rotor mass moment of inertia, rotor speed and tilt/yaw rotational velocity. For the two-bladed turbine, an extra effect to these loads is the varying rotor inertia depending on the azimuth position. The rotor inertia is significantly different around the pitch axis than any direction perpendicular to this. The different load

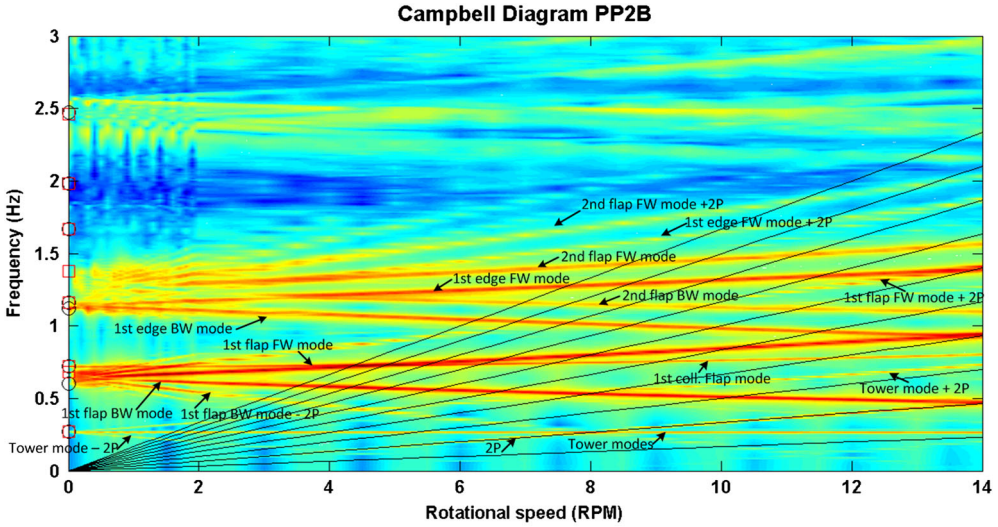

(a) Campbell diagram for PP-2B during the operation

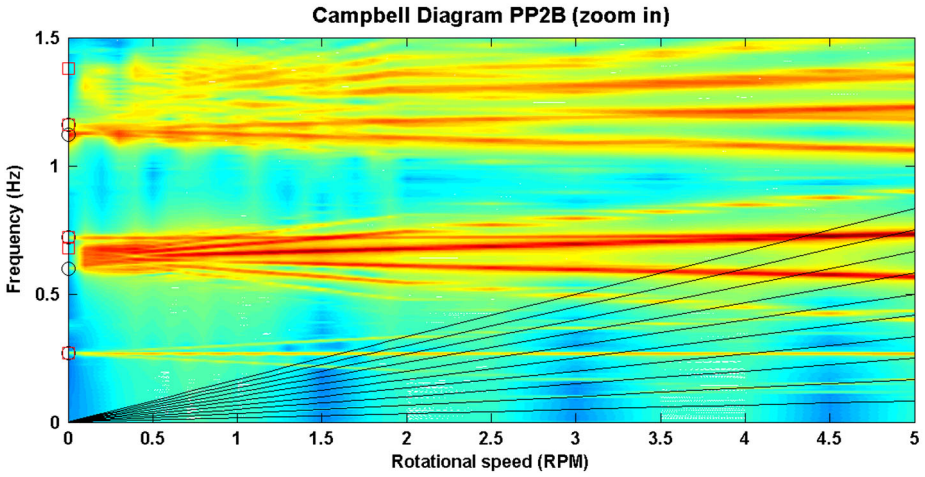

(b) Zoom in Campbell diagram for PP-2B

Figure 5. Structural frequency variation of the PP-2B turbine during the operation; the forward (FW) and backward (BW) whirl modes of the flap and edge are spread with not only ±1P frequency but also multiple P frequency.

transferred to the tower during a yaw situation with constant yaw rate is shown in Figure 7. The rotor speed is fixed at 14 rpm. Nine different yaw rates were simulated from 0.1 to 0.9 ($^\circ\,s^{-1}$). All aerodynamic effects are disregarded. It is clearly seen from Figure 7(a) that the tower bottom torsion moment of the two-bladed turbine is rapidly increasing for increasing yaw rates, whereas the gyroscopic loads are not significant for the three-bladed turbine. Figure 7(b) and (c) show the tower top torsion moment in time for the PP-2B and the 3B turbine, respectively. For the three-bladed turbine (Figure 7(c)), the gyroscopic effects result in 3P sinusoidal yaw moments. For the two-bladed turbine, the gyroscopic effects result in a yaw moment mainly dominated by 2P, but higher harmonics are also present because of the non-sinusoidal shape.

4.4. Load comparison in operational conditions

The PP-2B turbine loads in the operational conditions are compared with the PP-3B and the 3B turbines. For the statistical load comparisons, the normal operation at different wind speeds with a turbulence level according to class *IIB* is included in DLC 1.1, power production with electrical fault cases in which the turbine operates at 25 m s^{-1} with a mean yaw error of ±20° is included in DLC 2.4 and the normal operation with extreme turbulence intensity of 24.4% in DLC 1.3. Three different turbulence seeds are considered for each load case to account for some statistical variation. All values are normalized with an absolute value of the minimum out-of-plane blade root bending moment at 11 m s^{-1} (Figure 11) except for the electrical

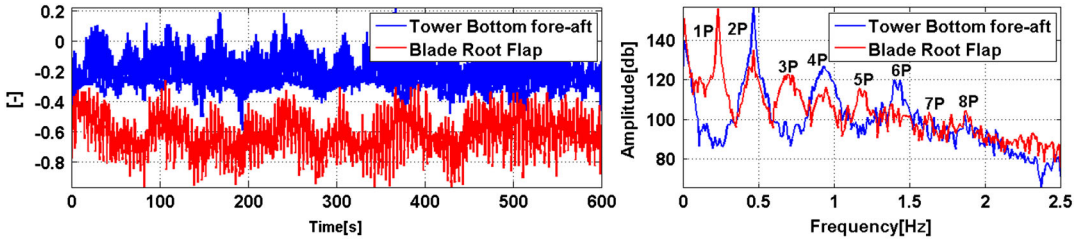

(a) Tower root bending moment vs. blade root flapwise bending moment for the PP-2B turbine at 11m/s.

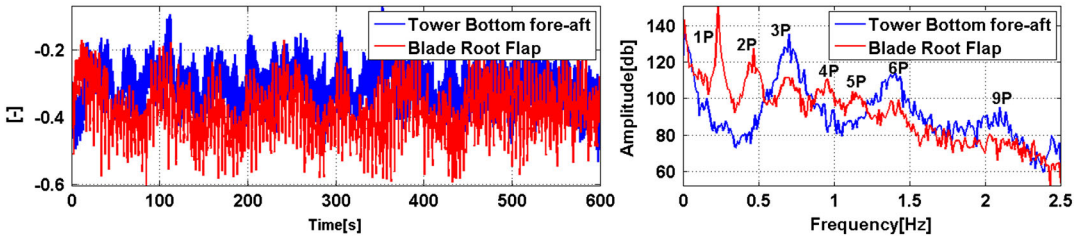

(b) Tower root bending moment vs. blade root flapwise bending moment for the 3B turbine at 11m/s

Figure 6. Two- and three-bladed turbine dynamic behavior in time and frequency domain. All values in time domain are normalized with the absolute value of the minimum out-of-plane blade root bending moment at 11 m s^{-1} (Figure 11).

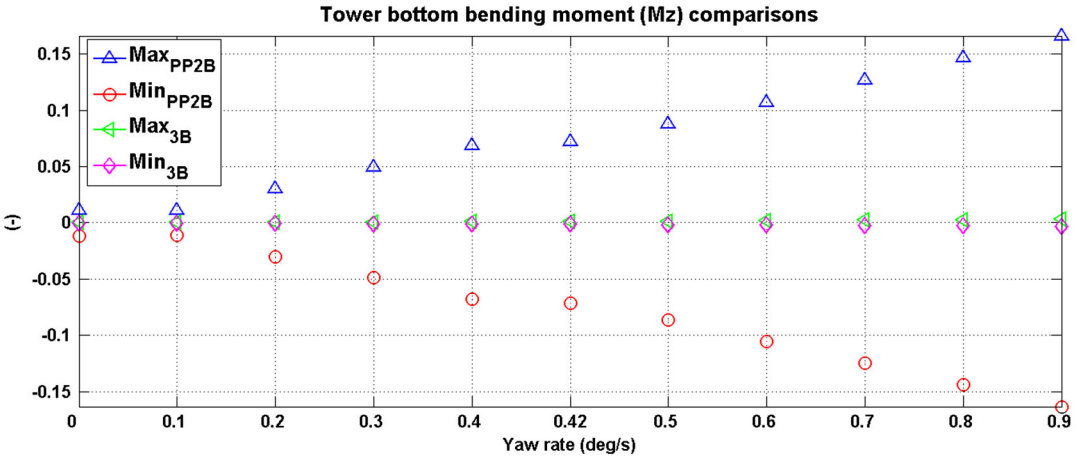

(a) Gyroscopic load comparison for PP-2B (blue Δ and red ○), and 3B (green Δ and pink ◊). Tower bottom torsion (M_z) is compared by increasing yaw rate from 0 to 0.9 deg/sec.

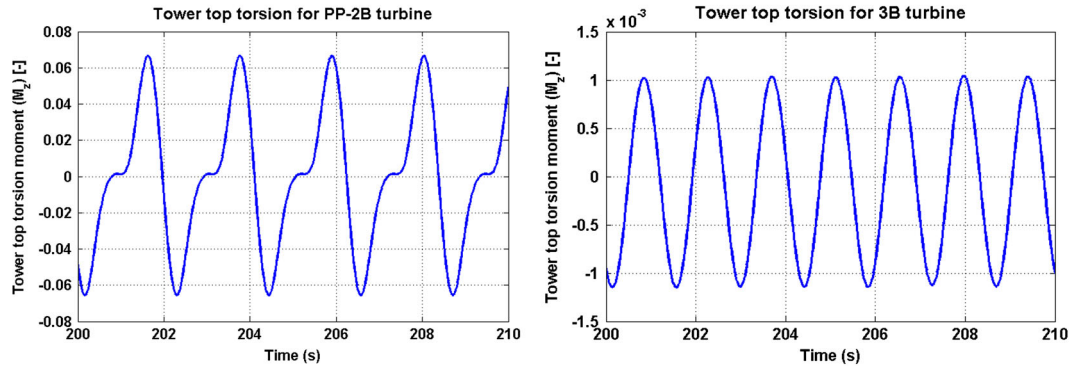

(b) Tower top torsion moment for PP-2B in time domain.

(c) Tower top torsion moment for 3B in time domain.

Figure 7. Gyroscopic load comparison for PP-2B and 3B; notice the difference in absolute load level on the *y*-axis between (b) and (c). All values are normalized with the absolute value of the minimum out-of-plane blade root bending moment at 11 m s^{-1} (Figure 11).

power, the blade tip deflection (Figure 9(a)), the effective blade radius (Figure 9(b)), rotational speed and pitch angle, where the pitch angle is normalized with the maximum pitch angle (Figure 12).

When observing the power production for the three turbines in Figure 8, it can be seen that the mean power for all three turbines are almost identical. This may be a little surprising since a two-bladed turbine in general will generate less power than the three-bladed because of a larger tip loss effect. However, in this particular case, the increased tip loss is actually compensated by the increased blade stiffness causing a smaller effect from blade deflection. The blade deflection of the three-bladed turbine (PP-3B) is approximately 30% larger than for the similar two-bladed turbine (PP-2B), as seen in Figure 9(a). The blade deflection results in a reduced effective diameter, hence a reduced power production. From Figure 9(b), it has been shown that the PP-3B blades at all wind speeds have a smaller effective diameter than the one from the PP-2B. This effect is included through the non-linear structural formulation of HAWC2 taking the effects of large deflections and rotations into account, hence it will not be seen in, for example, modal-based aeroelastic codes. When observing the power output range below rated wind speed, it

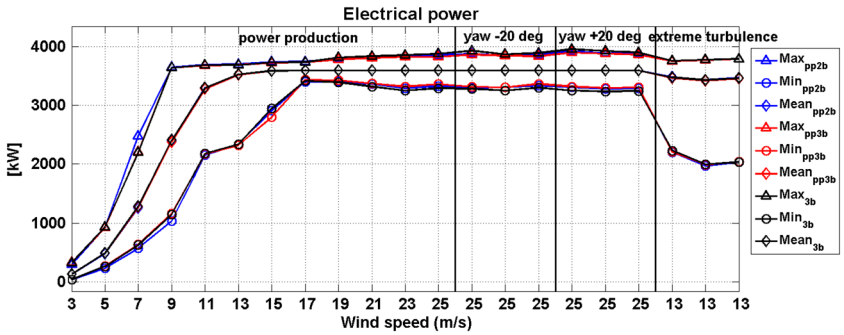

Figure 8. Generator power comparison for PP-2B (blue), PP-3B (red) and 3B (black).

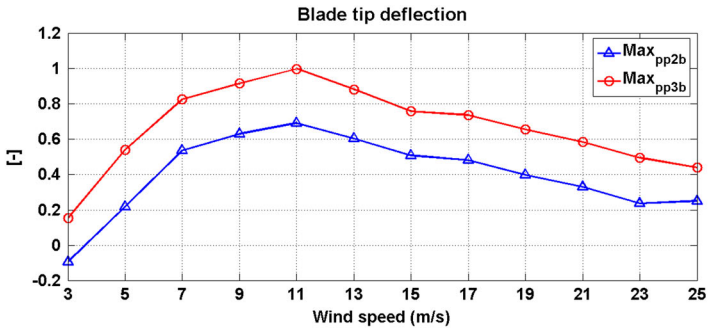

(a) Blade tip deflection comparison between PP-2B (blue Δ) and PP-3B (red ○). The blade tip deflections are measured on the pitch bearing and normalized with the maximum blade tip deflection of PP-3B turbine.

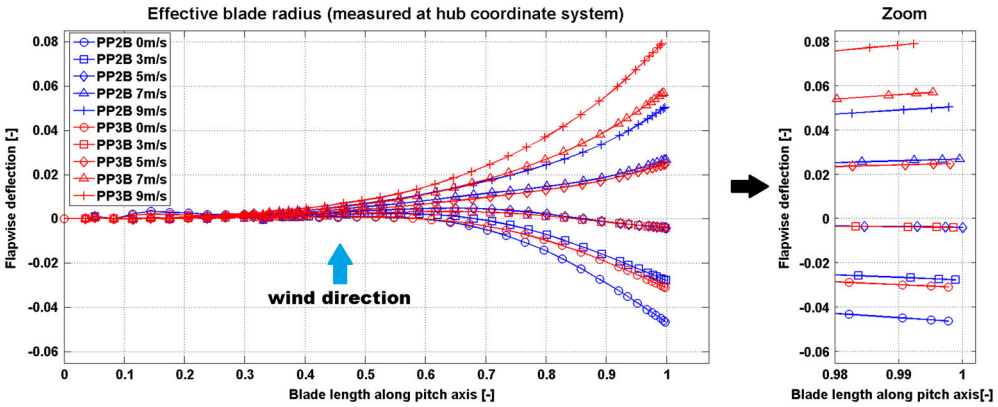

(b) Effective blade radius comparisons between PP-2B (blue) and PP-3B (red) with respect to different wind speeds. The mean effective blade radius are measured on the hub and normalized with the effective blade radius of PP-2B turbine at 5m/s (approximately 64.5m).

Figure 9. Blade tip deflection and effective blade radius comparisons between two- and three-bladed wind turbines.

can be seen that the power variation is slightly higher for the two-bladed turbine than the three-bladed. The reason for this is that the controller is not tuned specifically for the individual concepts. The exact same controller is used for all of the turbines. In this study, a proportional-integral-derivative (PID) controller developed by DTU Wind Energy is used.[17,37] The comparison of rotor speed is shown in Figure 10. The rated rotor speed is 14 rpm for all turbines. The mean values are all very similar.

The blade root out-of-plane bending moment for the turbines is shown in Figure 11. The bending moments for the PP-2B turbine are approximately 1.5 times larger than the PP-3B and the 3B turbines since the two blades carry the same aerodynamic load compared with the three-bladed turbines. The out-of-plane bending moment for the PP-3B is larger than the 3B beyond rated wind speed though they have the same number of the blades. This is caused by differences from the inner blade part, where the blade was originally designed to be stall-regulated, which means that a higher pitch angle is required for the 3B turbine in order to maintain a constant torque after rated wind speed (Figure 12).

The blade root in-plane bending moment for the turbines is shown in Figure 13. The in-plane bending moment of the PP-2B is larger than for the three-bladed turbines. The aerodynamic forces are roughly 3/2 times larger for the two-bladed than the three-bladed at all wind speeds, but since the blade weight is the same for all the concepts, the edgewise bending moment is only slightly different, which could be beneficial with respect to blade fatigue. The three-bladed turbines, PP-3B and 3B, show very similar in-plane moments as expected.

Lateral and longitudinal tower bottom bending moments for the three turbines are shown in Figures 14 and 15. In both figures, the considered wind speeds start from 9 m s^{-1} because of a tower 2P excitation at lower wind speed and corresponding lower rotor speed. In this region of low wind speed, the controller needs to be significantly different for the two- and three-bladed wind turbines in order to avoid resonance. However, it was chosen to leave out this wind speed range for the tower load comparison instead of operating with different control strategies for the two- and three-bladed turbines.

From Figure 14, the mean values of the lateral bending moment for all three turbines are seen to agree well. But the PP-2B has larger load variation because the 2P excitation is closer to the tower frequency than the 3P. Similar behavior is also observed at the longitudinal tower bottom bending moment in Figure 15. Interesting to notice, from the longitudinal tower bottom bending moment, is that the 3B turbine shows a lower mean bending moment above rated wind speed than the others. This is due to the difference in the aerodynamic loads of both inner and outer parts due to different pitch setting.

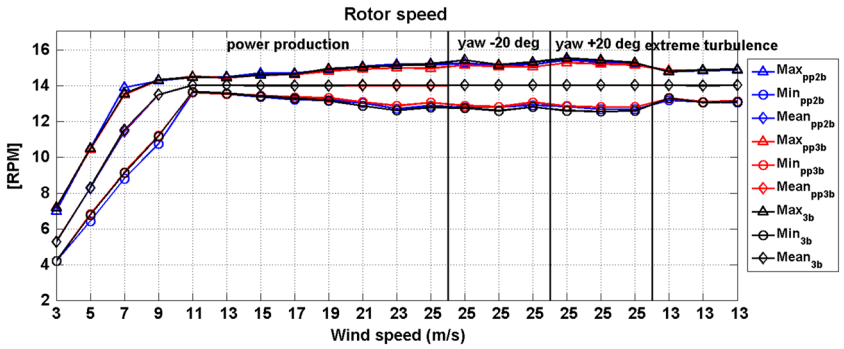

Figure 10. Rotor speed comparison for PP-2B (blue), PP-3B (red) and 3B (black).

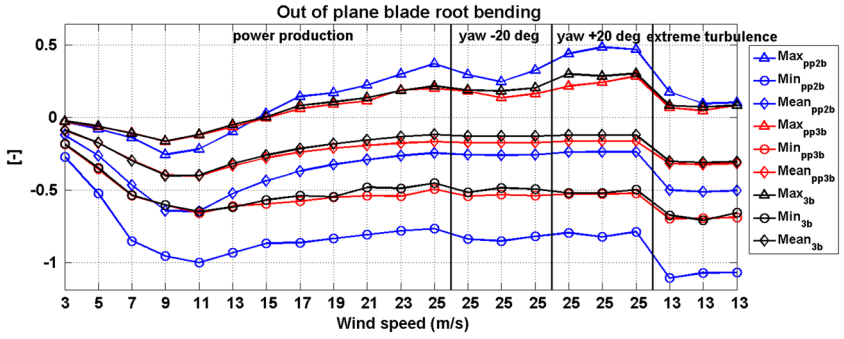

Figure 11. Out-of-plane blade root bending moment comparison for PP-2B (blue), PP-3B (red) and 3B (black). All values are normalized with the absolute value of the minimum out-of-plane blade root bending moment at 11 m s^{-1}.

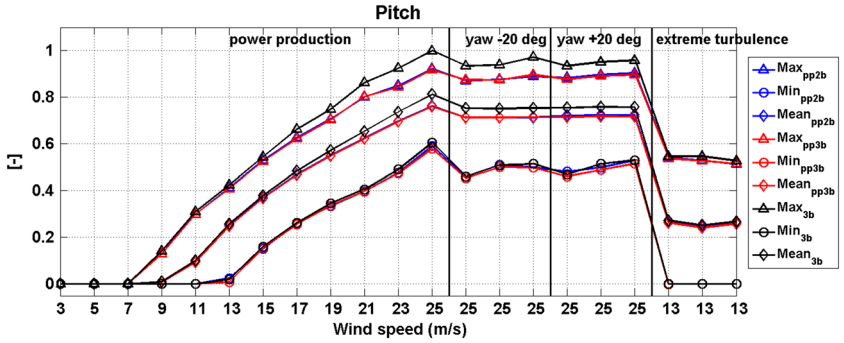

Figure 12. Pitch action comparison for PP-2B (blue), PP-3B (red) and 3B (black). All values are normalized with the maximum pitch angle of the 3B.

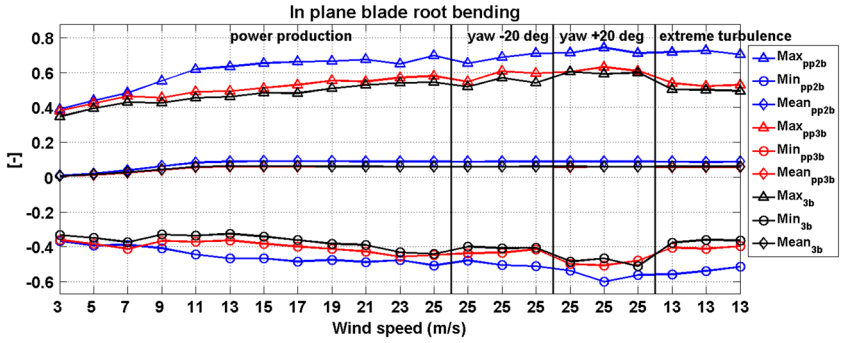

Figure 13. In-plane blade root bending moment comparison for PP-2B (blue), PP-3B (red) and 3B (black). All values are normalized with the absolute value of the minimum out-of-plane blade root bending moment at 11 m s^{-1} (Figure 11).

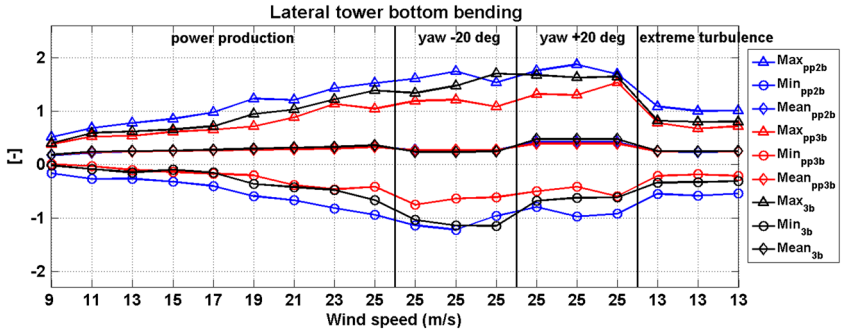

Figure 14. Lateral tower bottom bending moment for PP-2B (blue), PP-3B (red) and 3B (black). All values are normalized with the absolute value of the minimum out-of-plane blade root bending moment at 11 m s^{-1} (Figure 11).

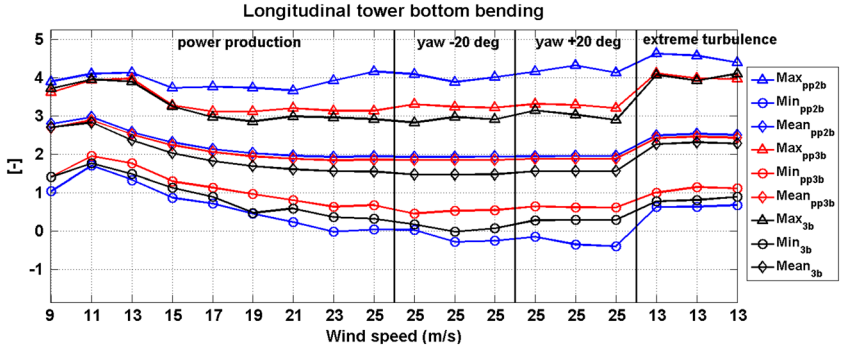

Figure 15. Longitudinal tower bottom bending moment comparison for PP-2B (blue), PP-3B (red) and 3B (black). All values are normalized with the absolute value of the minimum out-of-plane blade root bending moment at 11 m s^{-1} (Figure 11).

4.5. Load comparison in extreme condition

One of the extreme load situations, which is particularly important for the motivation for the PP-2B concept, is the standstill storm event covered in DLC 6.2. It is clear that other load cases during operation in abnormal wind conditions or in combination with fault situations may also create large or even extreme loads, but as a first order estimate, these load cases may not in principle differ between the concepts as for the DLC 6.2. In this situation, all turbines are in standstill condition with the blades pitched 90° toward feather and with the shaft fixed in rotation. The blades of the PP-2B are horizontally placed (T-configuration). The wind direction covers all directions with an interval of 15°. The inflow angle is positive when the wind comes from the right seen from the turbine. Each load case is simulated with nine different turbulence seeds.

The tower bottom bending moment in the direction of the wind, called downwind tower bending moment, is shown in Figure 16(a) as function of wind direction. It is mainly dominated by drag driven forces on the blades and tower, where the blade loading depends on the angle of attack. This means that a wind direction of 0° results in larger loads for the partial pitched turbines (PP-2B and PP-3B) than for the 3B turbine, which is directly explained by a larger projected area of the

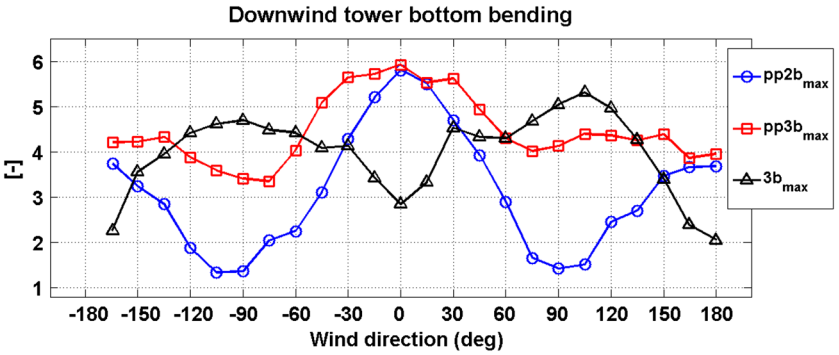

(a) Downwind tower bottom bending moment comparison

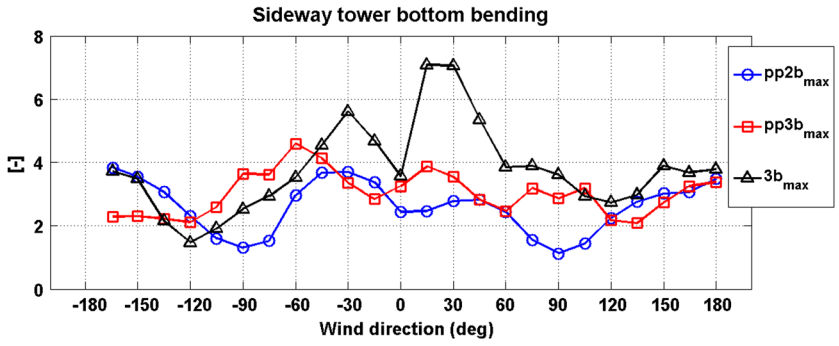

(b) Sideway tower bottom bending moment comparison

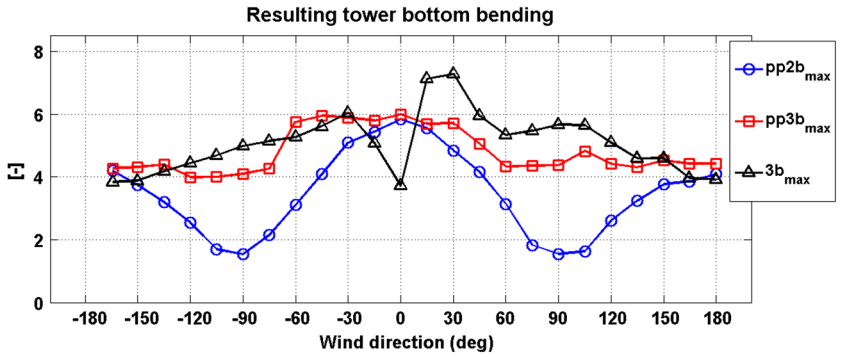

(c) Resulting tower bottom bending moment comparison

Figure 16. Tower bottom bending moment as function of wind direction. The turbine is at standstill. For the PP-2B (blue) parked in horizontal T-configuration, PP-3B (red) and the 3B (black). All values are normalized with the absolute value of the minimum out-of-plane blade root bending moment at 11 m s^{-1} (Figure 11).

inner blade part for this inflow angle. For the 3B turbine, the largest load occurs for an inflow angle around ±90°. The tower bottom bending moment for bending normal to the wind direction, called sideway tower bending moment, is shown in Figure 16(b), where the force is mainly dominated by lift driven forces on the blades and tower. The sideway tower bending moment is for some wind direction between 0° and 60° larger for the 3B than the partial pitch turbines. It is because the inflow angle gives the maximum angle of attack on the blade. On the other hand, the PP-3B and PP-2B experience bigger loads than the 3B for wind directions between −60° and −120° and between −120° and −175°, respectively. The largest resulting tower bottom bending moment, obtained as a square root summation of the fore-aft and side-side bending moment in time domain is shown in Figure 16(c). The maximum extreme load is approximately 20% lower for the PP-2B (0° wind inflow angle) and 18% lower for the PP-3B (0° wind inflow angle) compared with the 3B (30° wind inflow angle). Moreover, it is observed that the PP-2B has an even further potential for large reductions in the extreme tower load (more than approximately 60% extra load reduction) if wind directions between ±45° are avoided by a suitable parking strategy. Especially for wind direction of ±90°, the PP-2B provides a remarkably less tower bending moment compared with the three-bladed turbines (0° wind inflow angle for 3B and −120° wind inflow angle for PP-3B).

In order to show the importance of the azimuthal rotor position of the PP-2B, the resulting tower bottom bending moment with respect to the different blades positions is shown in Figure 17. Zero degree is with one blade positioned vertically downwards. When one blade is placed in between 60° and 120°, the partial pitch concept still has an advantage in terms of the extreme load reduction. However, if one blade is placed in between 0° and 30° or between 150° and 180°, the partial pitch concept is not beneficial. Therefore, it is necessary to ensure that the blades are positioned in between 60° and 120° by designing the controller to park in the T-configuration. It may also be possible to ensure this rotor position with different pitch setting on the blade such as 90° for the first blade and 85° for the second blade, enabling a different lift/drag on each blade.

The in-plane blade root bending moments are shown in Figure 18. It is seen that the PP-2B is less affected by the inflow direction than the PP-3B since the PP-2B is placed in the T-configuration. In contrast, the 3B turbine is strongly influenced by the wind direction. The largest load occurs for the 3B turbine, with a wind direction around 30° where the maximum angle of attack on the blade is obtained. It causes a full lift condition on the blade of the 3B turbine while the partial pitched blades avoid this full lift situation. Secondly, since the PP-2B turbine is placed in a T-configuration, the efficient projected

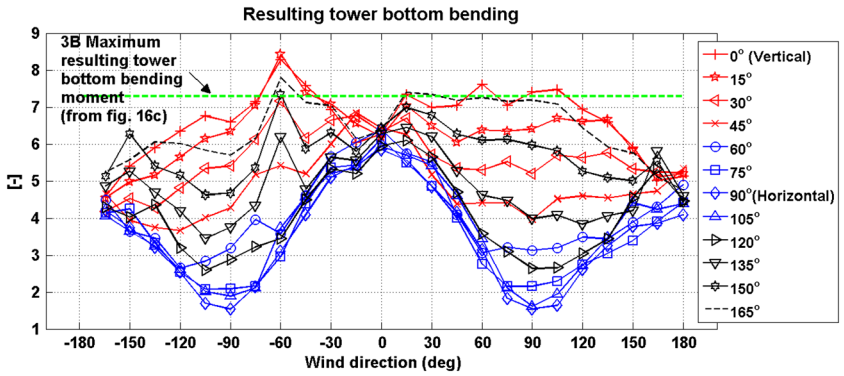

Figure 17. Resulting tower bottom bending moment depending on the azimuthal rotor position of the PP-2B. All values are normalized with the absolute value of the minimum out-of-plane blade root bending moment at 11 m s^{-1} (Figure 11).

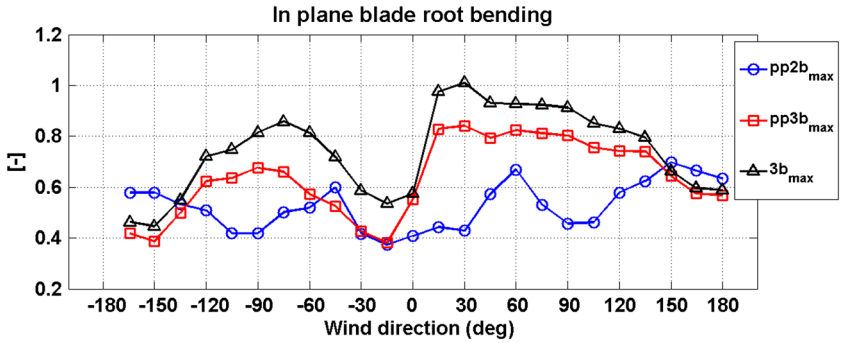

Figure 18. In-plane blade root bending moment comparison for PP-2B (blue), PP-3B (red) and 3B (black). All values are normalized with the absolute value of the minimum out-of-plane blade root bending moment at 11 m s^{-1} (Figure 11).

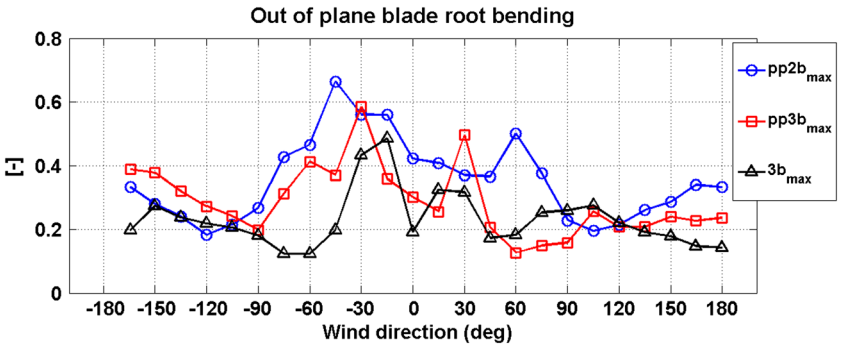

Figure 19. Out of plane blade root bending moment comparison for PP-2B (blue), PP-3B (red) and 3B (black). All values are normalized with the absolute value of the minimum out-of-plane blade root bending moment at 11 m s^{-1} (Figure 11).

blade area toward the wind is significantly reduced, depending on the wind direction which also reduces the loads. The out-of-plane blade root bending moments are shown in Figure 19. The load level of the out-of-plane blade bending moment is significantly lower than for the in-plane, caused by lower aerodynamic forces since the blade is pitched 90°. For a wind direction from 0°, the PP-2B turbine has the largest load compared with the others directly caused by the larger projected area of the inner part which is not pitched and therefore contributes with a higher drag level.

5. CONCLUSIONS

In this paper, three different turbines have been compared in order to examine the potential for an extreme load reduction with partial pitched blades and to compare principal differences between two- and three-bladed turbine dynamics with a rigid hub. From the partial pitch two-bladed (PP-2B) turbine, a partial pitch three-bladed (PP-3B) turbine and a normal fully pitch three-bladed (3B) turbine have been scaled on the basis of solidity similarity principles.

General dynamics of wind turbines with two and three blades were compared. The most dominating difference is the load transfer from the rotor to the tower where 2P and higher harmonic frequencies are excited in the tower by the two-bladed turbine, while a multiple of 3P excitation occurs in the three-bladed turbine. The structural frequencies during the operation were compared as well. A new and interesting finding is that the flap and edge related frequencies of two-bladed turbine were spread with ±1P frequency and multiple P frequency, whereas the frequencies are only spread with ±1P frequency for the three-bladed turbine. From the two-bladed turbine, it has been observed that the tower frequency is spread with ±2P frequency as well. The gyroscopic effect has also been investigated. For the two-bladed turbine, the tower bottom torsion is increasing more rapidly compared with three-bladed turbine when the yaw rate is raised. Gyroscopic loads during yaw operation are of limited importance for the three-bladed concept.

Several load cases were investigated to illustrate some key differences. Normal power production with normal turbulence (DLC 1.1) and extreme turbulence (DLC 1.3), power production with loss of electrical network (DLC 2.4) and parked with a loss of grid connection (DLC 6.2) are considered as the main DLCs. The blade load level is about 1.5 times higher for the PP-2B turbine directly caused by the 50% increased chord due to the solidity similarity, by handling the same amount of loads with one blade less rotor and by considering a rigid hub system. Larger tower load variations during operations were observed for the PP-2B turbine because of the 2P excitation from the rotor being closer to the tower frequency than 3P of a three-bladed turbine. The extreme tower loads during parked situation in a storm were reduced with around 20% and 18% for the PP-2B and the PP-3B compared with the 3B. Moreover, a huge potential of reducing the extreme load of 60% for the PP-2B could be obtained if the blades are placed in a T-configuration and perpendicular to the wind (wind direction of ±90°). Also, less blade root bending moments were observed from the PP-2B turbine for the standstill storm condition. In conclusion, the partial pitched blade is able to reduce an extreme load at the standstill storm situation when all wind directions are taken into account. Also the partial pitched blades experience less loading than the 3B turbine at the standstill condition. Moreover, the loading on the partial pitched blades are less affected by changes in wind direction during standstill condition.

ACKNOWLEDGEMENTS

This work is funded by the EUDP-2011 II project *Demonstration of Partial Pitch 2-Bladed Wind Turbine Performance*, which is gratefully acknowledged. Envision is also gratefully acknowledged for providing turbine information for this study.

REFERENCES

1. Hau E. *Wind Turbines: Fundamentals, Technologies, Application, Economics, Chapter 2*. Springer: Berlin, Germany, 2006.
2. Spera DA. *Wind turbine technology: Fundamental Concepts of Wind Turbine Engineering*. The America Society of Mechanical Engineers: New York, 1995.
3. Spera DA, Janetzke DC, Richards TR. Dynamic blade loading in the ERDA-NASA 100kw and 200kw wind turbines. *NASA TM-73711* 1977.
4. Linscott BS, Dennett JT, Gordon LH. The Mod-2 wind turbine development project. *NASA TM-82681* 1981.
5. General Electric Company. Mod-5a wind turbine generator program design report. DOE/NASA/0153-3, NASA CR-174736, August 1984.
6. Price TJ. UK large-scale wind power programme from 1970 to 1990: the Carmarthen Bay experiments and the Musgrove vertical axis turbines. *Wind Engineering* 2006; **30**: 225–242.
7. Maine International Consulting LLC. Floating Offshore Wind Foundations: Industry Consortia and Projects in the United States, Europe and Japan. An Overview, September 2012. http://www.maine-intl-consulting.com/
8. Sutherland HJ, Kelly ND. Inflow and fatigue response of the NWTC advanced research turbine. *ASME Wind Energy Symposium Technical Paper at the 41st AIAA Aerospace Science Meeting and Exhibit (Reno)* 2003.
9. Rasmussen F, Kretz A. A dynamics and potentials for the two-bladed teetering rotor concept. *Proc. AWEA Conf. (Seattle)* 1992.
10. Rasmussen F. Dynamics of a two-bladed teetering rotor. *Risø-R-617(EN)* 1992.
11. Kallesøe BJ, Helge AM, Larsen TJ, Rasmussen F. On the dynamics of a teeter hinge with delta 3 angle on a two bladed multi MW wind turbine. *Conf. Proc. 46th AIAA Aerospace Sciences Meeting and Exhibit (Reno)* 2008.
12. Larsen TJ, Madsen HA, Thomsen K, Rasmussen F. Reduction of teeter angle excursions for a two-bladed downwind rotor using cyclic pitch control. *Conf. Proc. 2007 European Wind Energy Conference and Exhibition (Milan)* 2007.
13. Kim T, Kallesøe BS, Friedrich M. Load reduction for a two-bladed upwind turbine with partial pitch. *Conf. Proc. EWEA offshore 2011 (Amsterdam)* 2011.
14. Poore R. NWTC AWT-26 research and retrofit project—summary of AWT-26/27 turbine research and development. *NREL/SR-500-26926* 1998.
15. Larsen TJ. Hansen AM. How to HAWC2, the users manual. Risø-R-1597(en) 2007.
16. Kim T. Hansen AM. Branner K. Development of an anisotropic beam finite element for composite wind turbine blades in multibody system. *Renewable Energy* 2013; **59**: 172–183. DOI:10.1016/j.renene.2013.03.033.
17. Larsen TJ. Madsen HA. Larsen GC. Hansen KS. Validation of the dynamic wake meander model for loads and power production in the Egmond aan Zee wind farm. *Wind Energy* 2012; Online available, DOI: 10.1002/we.1563.
18. Hansen MH. Gaunaa M. Madsen HA. A Beddoes–Leishman type dynamic stall model in state-space and indicial formulations. Risø National Laboratory, 2004, Risø-R-1354(EN).
19. Leishman JG, Beddoes TS. A generalized model for airfoil unsteady aerodynamic behaviour and dynamic stall using the indicial method. Proceeding of the 42end Annual Forum of the American Helicopter Society. 1986.
20. Theodorsen T. General theory of aerodynamic instability and the mechanism of flutter. NACA Report 435 1935: 413–433.
21. Madsen HA, Riziotis V, Zahle F, Hansen MOL, Snel H, Grasso F, Larsen TJ, Politis E. Rasmussen F. BEM blade element momentum modeling of inflow with shear in comparison with advanced model results. *Wind Energy* 2011; **15**: 63–81. DOI:10.1002/we.493.
22. Mann J. Wind field simulation. *Probabilistic Engineering Mechanics* 1998; **13**: 269–283.
23. Vorpahl F, Strobel M, Jonkman JM, Larsen TJ, Passon P, Nichols J. Verification of aero-elastic offshore wind turbine design codes under IEA wind task XXIII. *Wind Energy* 2013; online published, DOI:10.1002/we.1588.
24. Popko W, Vorpahl F, Zuga A, Kohlmeier M, Jonkman J, Robertson A, Larsen TJ, Yde A, Sætertrø K, Okstad KM, Nichols J, Nygaard TA, Gao Z, Manolas D, Kim K, Yu Q, Shi W, Park H, Vásquez-Rojas A, Dubois J, Kaufer D, Thomassen P, de Ruiter MJ, Peeringa JM, Zhiwen H, von Waaden H. Offshore code comparison collaboration continuation (OC4), phase I —results of coupled simulations of an offshore wind turbine with jacket support structure. *Proceedings of the 22nd International Society of Offshore and Polar Engineers Conference*, Rhodes, Greece, June 17-22, 2012.
25. Willson RE, Lissaman PBS. Applied aerodynamics of wind power machines. Origon State University, May 1974.
26. IEC61400-1. ed.3. Wind turbines Part 1: Design requirements. Technical report. International electrotechnical Commission 2005.
27. Petersen JT, Thomsen K, Madsen HA. Local blade whirl and global rotor whirl interaction. *Risø-R-1067(EN)*, Risø National Laboratory, 1998.

28. Hansen MH. Aeroelastic instability problems for wind turbines, *Wind Energy* 2007; **10**: 551–577.
29. Bossanyi EA. *GH Bladed Theory Manual*. GH & Partners Ltd: Bristol, England, 2003.
30. Øye S. FLEX4 simulation of wind turbine dynamics. In *Proceedings of the 28th IEA Meeting of Experts Concerning State of the Art of Aeroelastic Codes for wind Turbine Calculations*. Pedersen BM (ed.). Technical University of Denmark: Lyngby, 1996; 129–135.
31. Jonkman JM, Buhl ML Jr. FAST user's guide. *NREL/EL-500-29798*. National Renewable Energy Laboratory: Golden, Colorado, 2005.
32. Riziotis VA, Voutsinas SG. GAST: a general aerodynamic and structural prediction tool for wind turbines. *Proceedings of the EWEC'97*, Dublin, Ireland, 1997.
33. Hansen MH. Aeroelastic properties of backward swept blades. *Proceedings of 49th AIAA Aerospace Sciences Meeting Including The New Horizons Forum and Aerospace Exposition*, Orlando, January, 2011.
34. Floquet G. Sur les équations différentielles linéaires à coefficients périodiques. *Annales de l'École Normale Supérieure* 1883; **2**: 47–88.
35. Skjoldan PF. Aeroelastic modal dynamics of wind turbines including anisotropic effects. Risø-PhD-66(EN) 2011.
36. Burton T, Sharpe D, Jenkins N, Bossanyi E. *Wind Energy Handbook*. John Wiley & Sons: Chichester, 2001.
37. Hansen MH, Hansen A, Larsen TJ, Øye S, Sørensen P, Fuglsang P. Control design for a pitch-regulated, variable speed wind turbine. *Risø-R-1500(EN)*, Risø National Laboratory, 2005.